2023-XX-XXXX

Dynamic and Static Test Methods: Quantifying the Shear Strength at the Interface of Iced Substrates

Giulia Gastaldo†, Valerie Pommier-Budinger
ISAE-SUPAERO, Université de Toulouse, 10 Avenue Edouard Belin, 31400 Toulouse, France

Luca Stendardo†, Carlo Antonini, Anny Catalina Ospina Patiño
Department of Materials Science, University of Milano – Bicocca, via R. Cozzi 55, 20125 Milano, Italy

Marc Budinger
ICA, Université de Toulouse, UPS, INSA, ISAE-SUPAERO, MINES-ALBI, CNRS, 3 rue Caroline Aigle, 31400 Toulouse, France

Abstract

Surfaces with low ice adhesion are crucial for many technological and societal applications. However, comparing the performance of different surface coatings still represents a major challenge, given the broad range of ice accretion and removal conditions. One of the most common methodologies relies on measuring ice adhesion, which is often quantified by the shear strength of the ice-substrate interface. Nevertheless, large discrepancies up to one order of magnitude exist among the shear strength values reported in the literature for similar test conditions. This work compares shear strength measurements between two inherently different ice adhesion measurement techniques: (i) a dynamic, vibratory approach and (ii) a more traditional static push test on a horizontal surface. By employing a hybrid experimental and numerical approach, the shear strength is obtained for both techniques. This approach allows a direct correlation between a low-complexity static setup and a dynamic test rig, close to the operating conditions of vibratory applications but more challenging to implement. As such, this study enables a better understanding and design of ice adhesion measurement procedures for testing both traditional and icephobic surfaces.

Introduction

Ice accretion has a negative impact on wind turbines [1, 2], energy infrastructures (i.e. electric transmission lines [3]), aviation [4], and many more systems operating in cold climates. It causes losses in performance, and it compromises the safety of the aforementioned systems. Regarding turbine blades and aircraft wings, the accreted ice modifies the airfoil shape, leading to severe degradation of the aerodynamic properties [5]. Such issues are addressed by using ice protection systems (IPS), which traditionally rely on chemical, thermal, and mechanical approaches [6], [7]. In recent years, electromechanical IPS have gained increasing interest due to their weight and energy savings potential. These systems incorporate piezoelectric actuators, which excite the surface covered by ice with vibrations. They generate a resonant response of the ice and, therefore, high stresses, ultimately leading to ice detachment [8], [9] [10]. Piezoelectric actuators can also be coupled with passive solutions preventing ice adhesion (i.e. icephobic coatings) to increase protection from ice.

Ice forming in atmospheric conditions is generally classified into three categories: in-cloud icing, precipitation icing, and hoarfrost [11]. Additionally, ice can also be classified depending on its type and properties, namely glaze ice, rime ice, snow, or frost [12]. Densities from 150 kg/m^3 to 900 kg/m^3 can be measured in this broad range of ice types. Given that electromechanical ice protection systems rely on the mechanical resonance of the ice layer, having adequate information on the mechanical properties of the ice constitutes a priority to ensure effective de-icing. Additionally, ice fracture propagation at the interface with the substrate is closely related to the fracture toughness and the adhesive strength of ice. Hence, both the mechanical and the interfacial properties play an essential role when dimensioning the power requirements of the system.

The large number of technological applications where icing is problematic has led to many studies on the characterization of ice adhesive properties. In [13], a critical review of the broad range of mechanical and adhesive properties of ice has been presented. The observed discrepancies among tests on similar surfaces may be due to different freezing conditions and the adopted measurement techniques. For example, the data collected from 52 studies show that the ice adhesion strength generally increases with decreasing temperature. The same work analyses the relationship with water-impact velocity, reporting reduced adhesion strength for higher impact velocities. Tarquini et al. [14] investigated the influence of the droplet median volumetric diameter (MVD), showing a decreasing adhesive strength with increasing MVD. In the same work, the influence of the liquid water content (LWC) was investigated, showing a non-monotonic trend: ice shedding stress increases approximately for LWC from 0.5 to 2 g/m^3, which are representative values for the icing envelope. In this regard, Rønneberg et al. [15] studied the influence of ice type on adhesive strength. The three different types of ice (precipitation ice, impact ice from in-cloud icing and bulk ice) were represented by their apparent density, which is the ratio of the ice mass to the thickness. It was noticed that the ice adhesion strength is higher for lower ice densities. The authors justify this phenomenon by correlating the density and the grain size. Higher ice densities generally correspond to larger ice grain sizes that reduce the ice adhesive strength. Larger crystal grains are subject to higher stress concentrations, inducing micro-cracks at the interface and therefore lowering the overall measured ice adhesion strength.

Reviews of the experimental methods developed to measure the bond strength between ice and substrate have been conducted both by Rønneberg et al. [16] and by Work and Lian [13], identifying three major categories: (i) shear tests (including horizontal shear tests [17, 18, 19], vertical shear tests [20, 21, 22], rotational shear tests [23, 24], and zero degree cone tests [25, 26]), (ii) tensile tests [27, 28, 29], and (iii) centrifugal tests [15, 30, 31]. A wide range of research groups has utilized the above three methods, which are often employed for independent third-party validation. However, there is no straightforward way of comparing the performance of different ice adhesion test methods [32]. Each measurement method is usually suitable for a specific ice accretion or removal condition, but transferring and comparing results from one measurement method to another is far from trivial. Generally, the closer an experimental ice adhesion setup is to the final de-icing system, the more complex and cost-intensive it

is [32]. So, there is a practical and economic reason to correlate results from low-complexity static experimental methods to the results of dynamic ones, closer to the targeted applications such as airfoil resonant ice protection systems, but more complex to implement. This study compares adhesion strength measurements between static and dynamic experimental techniques. The static system used for this comparison is one of the most common laboratory-scale ice adhesion measurement setups: the horizontal push (or shear) test with freezer ice[33]. The dynamic experimental method used to investigate ice adhesion is a vibratory approach developed in [34] to measure the cohesive strength and the fracture toughness, extended here to measure the shear strength. Tests will be performed in similar conditions as that of the static tests to allow comparison of the results.

Measurement principles and setup descriptions

Dynamic Method

The dynamic method for ice detachment, introduced by Palanque et al. [34, 35], is based on vibratory studies and fracture propagation analyses carried out both numerically and experimentally on a titanium plate entirely covered with an ice layer. In [34], the goal was to retrieve two mechanical properties of the ice following the excitation of a resonant mode: the cohesive tensile strength of the ice and the adhesive fracture toughness required to propagate an already present cohesive crack.

In this study, the objective is to extend this dynamic method to retrieve the value of the shear strength at the interface between the ice layer and a certain substrate. To this end, adhesive failure needs to be triggered experimentally.

Test Rig Description

The experimental setup comprises a plate-like substrate (possibly covered with a coating) with a piezoelectric actuation system (e.g. piezoelectric plates bonded to the substrate) to vibrate it. The plate is installed in a freezer, where glaze-like ice can form (see Figure 1). Ice is accreted on the side of the plate opposite to the side where the actuation system is glued. The setup also comprises a laser vibrometer to measure the oscillation magnitude. This dynamic approach presents some constraints related to the use of the laser vibrometer (having an operating temperature range from +5°C to +40 °C) to retrieve the vibratory amplitude, while simultaneously preserving the iced sample at low temperatures (with a freezer temperature of -20°C). For this reason, an insulating layer (Styrodur) was tailored for the freezer, allowing the laser to be positioned on top, outside the chamber. A small window (10 x 10 cm²) was created to allow the laser measurements, and wooden rods were employed to suspend the plate and enable free vibrations. A picture of the setup is shown in Figure 2.

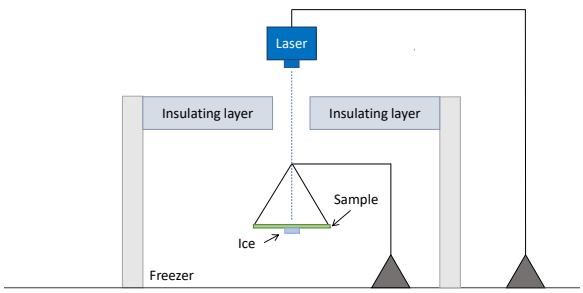

Figure 1: Schematic of the dynamic setup. The sample is kept horizontal by flexible wires, which ensure free boundary conditions

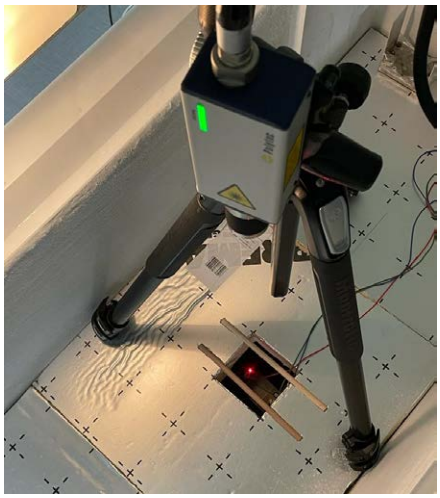

Figure 2: View of the dynamic test rig. The laser vibrometer is positioned in the freezer on top of the insulated layer, and pointing at the sample antinode to retrieve the displacement.

Measurement Principle

The sample is vibrated at one of its resonance frequencies to amplify its oscillations. At the moment the ice detaches, the resonant frequency of the system and the magnitude of the vibrations at the antinode (where the amplitude is the greatest) are measured. Then, a numerical analysis is run in the same vibratory conditions, from which the numerical displacement at the antinode x_{num} and the value of shear stress τ_{num} at the interface are retrieved. According to [36, 34], the experimental values for the modal amplitude and stresses can be obtained by linearly rescaling the numerical ones. Hence, knowing x_{num} and τ_{num}, as well as the experimentally measured displacement x_{exp} at the antinode (retrieved using the laser vibrometer), it is possible to obtain the value of the experimental shear stress τ_{exp}:

$$\tau_{exp} = \tau_{num} \frac{x_{exp}}{x_{num}} \tag{1}$$

Since the experimental shear stress is obtained at the time in which shedding occurs without the appearance of any cohesive cracks, this value corresponds to the shear strength of the ice-substrate interface τ_c.

The computation of the shear strength does not depend on the iced area if the size of the iced block is small enough to be in the conditions of a shear-dominated detachment. The condition is found for ice blocks of smaller dimensions, as explained in [37] and in the following paragraph.

Requirement for the dynamic method

It is important to control the fracture propagation mechanisms to ensure a good measurement of the shear strength. Depending on the chosen experimental configurations, these mechanisms can vary. Using a horizontal push test, Golovin et al. [18] identified two adhesive fracture mechanisms based on the size of the examined ice block. The authors were able to assess that, for small bonded lengths, fracture occurs when the average shear stress at the interface exceeds the shear strength $\tau_{xy} \geq \tau_c$ whereas, for long ice blocks, the fracture is dominated by the critical energy release rate $G \geq G_c$.

For dynamic tests, the fracture mechanisms of the ice layer were studied in [37]. It was found that, if the surface is largely covered with ice (long ice blocks), the fracture appears first in the ice bulk (cohesive fracture) and then propagates at the ice/substrate interface, by exceeding first the fracture toughness of the interface and, secondly, above a certain crack length, the shear strength. For ice blocks below a certain

critical length (short ice blocks), there are no cohesive fractures, but only adhesive fractures induced by exceeding first the fracture toughness of the interface and secondly the shear strength. If the ice blocks are very small and close to the nodes, the shear strength criterion is met before exceeding the critical fracture toughness. Therefore, delamination is only controlled by shear stress.

To obtain the characteristic value of shear strength for a certain ice/substrate interface, it will thus be necessary to be in a configuration in which pure shear detachment is ensured. Therefore, it is of utmost importance to choose a proper combination of the resonant mode, the relative position of the ice block to the nodes and the size of the ice layer.

Choice of the Resonance Mode

The choice of the resonant mode and the size of the ice block enabling adhesive shear detachment are investigated numerically. The plate under study is a titanium plate of dimension 130x50x1 mm^3. According to [37], shear-dominated detachment (appearing as instantaneous delamination) is observed for small ice blocks. Therefore, a small ice block of surface 8x8 mm^2 and height 5 mm is chosen a priori for the experimental study. Numerical computations are run to verify that detachment occurred under shear stresses.

For the shear-dominated detachment to occur, the stress distribution at the interface has to be as uniform as possible. A 2D study is run on the titanium plate of 130 x 1 mm², presenting an ice layer (8 x 5 mm²) located in the middle. The modal analysis is run in free boundary conditions with a mesh size fine enough to ensure the convergence of the results. The first four flexural modes are observed in the range [281-2450] Hz.

The stress distributions for the different modes were compared by analyzing the ratio $\tau/\sqrt{P}$ which is independent of the operating point and where τ corresponds to the stress along the interface and P to the mechanical power per unit area required to vibrate the plate and computed as in [36]:

$$P = \frac{1}{2A} F\dot{x} = \frac{1}{2A} \frac{K_{eq} x^2 \omega}{Q_m} = \frac{1}{2A} \frac{U\omega}{Q_m} \tag{2}$$

In equation 2, A is the surface area of the considered plate sample, U the strain energy of the mode under consideration, ω its angular velocity, and Q_m its quality factor which was set to an average value of 50. For the first four flexural modes, the ratio $\tau/\sqrt{P}$ is plotted in Figure 3. It is reported around the ice/substrate interface, thus around 65 mm since the ice is placed in the middle of the plate. All the analyzed modes presented edge effects, represented by the peaks in value of $\tau/\sqrt{P}$ of the opposite sign to the values in the central part. These peak stresses observed at the sharp edges are considered numerical artifacts with no physical effect. Thus, the edge effects were neglected in calculating τ_{num}.

For the modes having an antinode at the plate center (i.e. modes 1 and 3), the stress distribution was less uniform and presented a value equal to zero at the center. Conversely, modes with a node located in the middle (i.e. modes 2 and 4) presented a more uniform stress distribution. As such, the second flexural mode was chosen for the experiments.

To validate the previous results, a 3D numerical study is run for the second flexural mode with an ice block of size 8x8x5 mm^3 (Figure 4). The shear stress distributions at the interface/substrate are analyzed for different mesh refinements until mesh convergence is reached. The 3D study confirms the choice of the second resonance mode and the small ice block to get pure shear stress detachment.

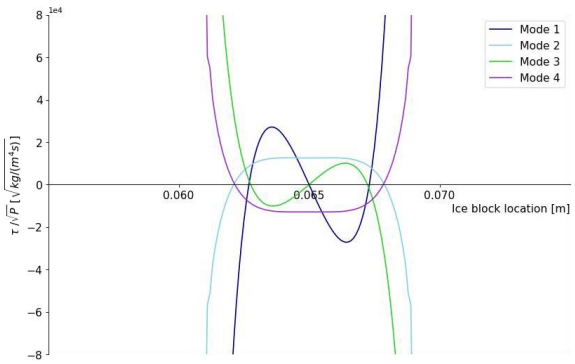

Figure 3: Ratio $\tau/\sqrt{P}$ at the interface ice/substrate for the first four resonant flexural modes. The ice block is located at the center of the plate (65 mm).

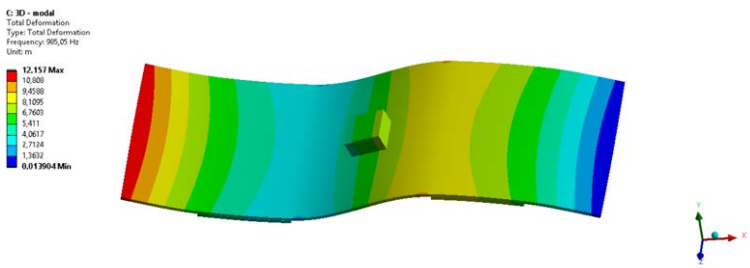

Figure 4: Second flexural mode for the titanium plate with an 8x8x5 mm^3 ice block accreted at the center.

Static Method

The static testing method used for this study is the horizontal push test [Fig. 5(a)]. For a pure shear test, the force needs to be applied tangential to the substrate, with the force probe placed as close as possible to the substrate [Fig. 5(b)]. A force that is applied at a finite height from the substrate (distance d) and parallel to it induces a mixed loading state, where shear, as well as tensile stress, is acting at the ice-substrate interface. The study of Maitra et al. [27] attempts to investigate the presence of a mixed shear/tensile loading mode at the ice-substrate interface. According to the authors, in the mixed loading state, the tensile stress σ has been measured to be consistently higher than the shear stress τ [27]. The height from the substrate at which the force is applied is, therefore, an important parameter when performing this kind of static shear test, as it can substantially alter the stress components at the ice-substrate interface. For this reason, the distance d will be minimized ($d \leq 1$ mm) to ensure a τ dominated ice detachment.

Test Rig Description

The static ice adhesion tests are performed using an in-house designed chamber [Fig. 6(a)]. The sample surface is clamped onto a cooling stage, which consists of a liquid-cooled heat sink with copper serpentine, two thermoelectric cells and an aluminum plate, which serves as a sample holder [Fig. 6(b)]. An environmental chamber is used to reduce humidity by continuous dry nitrogen supply (ambient temperature 20°C, relative humidity $< 3\%$), thus avoiding frost formation during freezing and testing.

The sample surface temperature is set to -20°C during the ice adhesion tests and controlled by a PID-Controller and a 5K-Ω thermistor (Te Technology, Inc.). A cylindrical nylon (PA.6) mold (inner diameter 8 mm, outer diameter 12 mm, and height 20 mm) is placed on the sample and filled (up to 8-10 mm) with deionized water ($T_{water} \approx 0$ °C). At

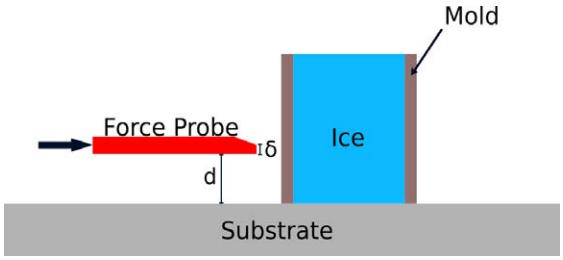

(a)

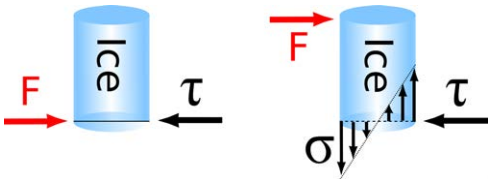

(b)

Figure 5: a) Schematic of the common horizontal push test. The ice is generally formed by pouring water inside a cuvette or mold in contact with the cooled substrate. A force probe (contact face size δ) is then pushed against the mold containing the ice at a distance d from the substrate. b) Depending on the distance d at which the force is applied on the ice, different loading states can be established at the ice-substrate interface. A tangential force creates a shear-dominated loading state, while a force parallel to the substrate generally induces a shear/tensile mixed loading state.

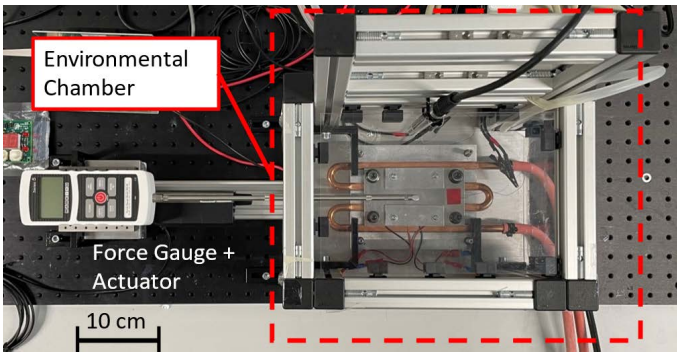

(a)

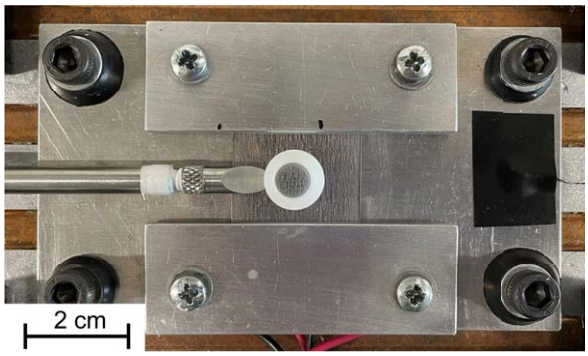

(b)

Figure 6: a) Top-view of the horizontal shear stress. Nitrogen gas flows into an environmental chamber, which is used to avoid frost formation during ice accretion and testing. A force gauge mounted on a linear actuator is used to detect the maximum adhesion force of the ice sample. b) Detail view of the sample cooling system. A cylindrical Nylon mold contains the water frozen by two thermoelectric elements placed under the sample holder.

least 20 min of conditioning time is given to ensure that the water column is completely frozen. Sealing the mold to the substrate is not necessary, as the water starts to freeze almost instantly when poured inside the mold. A visual inspection of the mold after each test is performed to ensure that no water has leaked under the mold during the freezing process. The pushing force is applied on the mold by a metallic rod and is measured by a force gauge (Mark-10 model M5-20, $F_{max} = 100$ N, Resolution $= 0,02$ N, last calibration on 20/09/2021) that is mounted on a linear displacement stage (Newport LTA-HL with Conex-CC Controller). Typically, ice molds with a square cross-section are employed with the horizontal push test [33, 18, 38]. In this study, a circular cross-section is used, which improves the alignment between the pushing rod and the ice column. The contact point between the pushing head and the mold is always located on the symmetry line of the ice column, reducing the alignment errors without the need for any special adjustments by the user of the test system. Therefore, this configuration is expected to minimize the deviation of the adhesion measurements but also to increase the stress concentrations in the ice near the contact point. During the testing of the samples, however, no cracking or cohesive failure of the ice was observed. The force sensor rod has access to the ice column by an opening in the chamber wall. A wedge-shaped head with a flat bottom side is mounted on the rod to ensure that the mold containing the ice is pushed close to the substrate ($d \leq 1$ mm). The linear actuator moves with a constant velocity of 10 µm/s, implying that the ice column's force increases with time after contact. The detected maximum force at the moment of adhesive failure is divided by the projected ice-substrate contact area to calculate the mean ice adhesion stress τ_{avg} (see Eq. 3), which in this study is assumed to correspond to the adhesive strength $\tau_c = \tau_{avg}$.

$$\tau_{avg} = \frac{F_{max}}{A} \tag{3}$$

Materials

Two titanium (TA6V) plates were used in this study to perform the tests. One plate was left uncoated, while on the other one a commercially available hydrophilic low-friction coating was applied (Oerlikon Dylyn). The coating is composed of an amorphous carbon material (a-C:H:Si) and it has been applied on the titanium substrate by Plasma-Assisted Chemical Vapor Deposition (PACVD). According to the manufacturer, this results in a H_{IT} coating hardness of 15-25 GPa and a dry friction coefficient of 0.05 - 0.2. In light of the low friction coefficient, it was expected that the adhesion strength of the Dylyn coating was lower than that of the bare titanium substrate. Moreover, the roughness of the two samples was measured using a profilometer (Veeco Dektak 8). It resulted in a roughness value of $R_a = 0,49\mu m$ for the uncoated titanium sample, while the coated sample presented a roughness of $R_a = 0,20\mu m$. Again, the roughness values supported the hypothesis of a lower ice adhesion value for the coated sample.

Results and Discussion

Samples testing

Two sample titanium alloy plates (TA6V) with the dimensions of 130x50x1 mm^3 were manufactured. Both were equipped with soft piezoceramic transducers (PIC 255, 25x50x1 mm^3) as in Figure 7(a). The piezoceramics were located at the antinodes of the second flexural mode. The first sample plate was uncoated (bare titanium), while the second one was coated with a low-friction coating (Oerlikon Dylyn). The ice block (8x8x5 mm^3) was accreted in the freezer at -20 °C using demineralized water and located at the center of the plate by using a flexible mold (Figure 7(b)). The conditioning time was at least 30 minutes. The ice is accreted in the form of bulk ice, and its density is comparable to the ice used in the push test (around 900 kg/m^3).

The dynamic experimental tests were conducted by exciting the second flexural mode. From these experiments, it was possible to observe instantaneous full delamination of the ice block, which indicates that the shear stresses at the interface exceed the shear strength that charac-

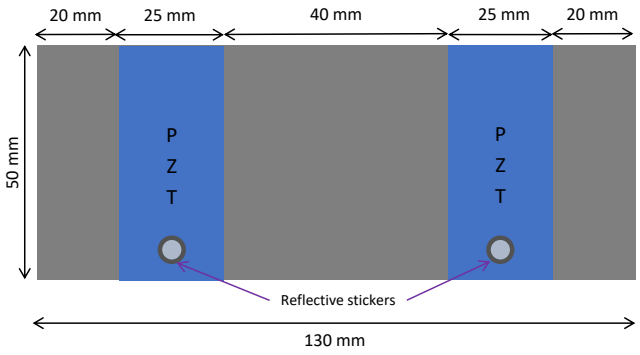

(a)

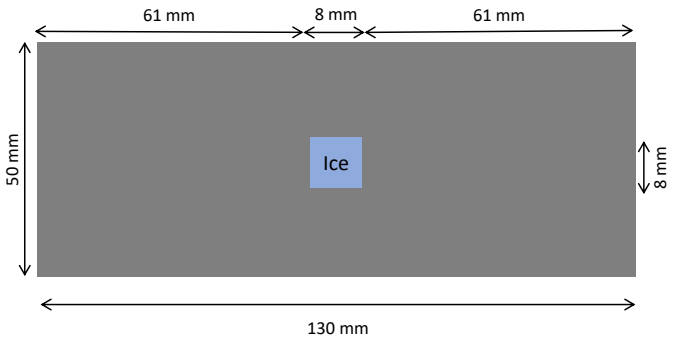

(b)

Figure 7: a) Rear view schematic of the plate. The piezoelectric transducers were located at the antinodes of the mode, and the reflective stickers were positioned in correspondence to the preferred pointing location of the laser. b) Front view schematic of the plate. The ice block (8x8x5 mm^3) was accreted in the freezer at -20 °C and located at the center of the titanium plate.

terizes the ice-substrate interface [37].

The displacement measurements were carried out using the setup displayed in Figure 2. The laser vibrometer was pointed towards a location on the centerline of the piezoelectric transducer to obtain the oscillation amplitude (x_{exp}). At the same time, the numerical analysis was performed. The numerical value of the shear stress τ_{num} was obtained by computing the average over the interface without considering the edge effects that were shown previously. The numerical displacement x_{num} was retrieved at the same location as in the experiment.

To accurately measure the oscillation speed that leads to the detachment of the ice block, it is important to gradually approach the resonant frequency of the plate with the ice block. Resonance cannot always be found at the same frequency due to minor differences in the ice block shape between measurements. To overcome this issue, a frequency sweep at high voltages close to the resonance was performed until the ice block detached from the substrate. Figure 8 shows an example of the oscillation speed measurement with the laser vibrometer (y-axis) as a function of the excitation frequency (x-axis) for the titanium sample.

In this example, a downward frequency sweep (from the highest frequency to the lowest one) has been performed. It can be seen how the oscillation speed increased gradually as the frequency approached the resonance frequency at around 1050 Hz. At this point, the ice block detached suddenly from the titanium plate, which can be seen from the drop in the oscillatory speed. After ice detachment, the mechanical

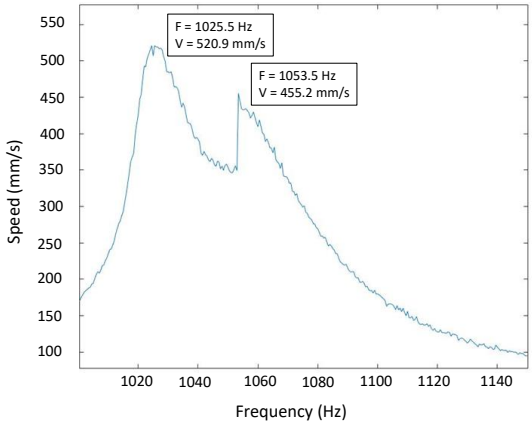

Figure 8: Oscillation speed *V* vs. excitation frequency *F*. A downward frequency sweep was performed until the ice block detached (first drop of *V* at about 1050 Hz). At this point, the frequency and oscillation speed were recorded and used to calculate τ_{exp} with the numerical model.

properties of the vibrating plate change slightly due to mass reduction, resulting in a different resonant frequency. Consequently, by continuing the sweep, it can be seen how the titanium plate reached a second shifted peak at around 1025 Hz. The frequency *F* and oscillation speed *V* at the moment of the detachment of the ice were recorded and used in the numerical model to retrieve the experimental shear strength τ_{exp}.

The complete measurements were presented in Figure 9. At least eight measurements were conducted for both substrates and both test methods. It can be seen how the shear strength is varying consistently between the two measurement methods. To understand the discrepancies in the values, it is necessary to evaluate them separately. In the case of the adopted static measurement method, traditionally the shear strength is calculated as τ_{avg} (see Eq. 3). As the ice is loaded locally, major stress concentrations close to the loading point are introduced at the ice-substrate interface. This is highlighted by Work and Lian in [13]. It can be seen how the maximum shear stress value along the interface is approximately seven times higher than the minimum value. In a stress-dominated regime, the stress level has to exceed the critical value over the entire interface [39, 40]. However, the τ_{avg} is overestimating the shear strength of the ice-substrate interface in the presence of such high stress concentrations.

The dynamic measurements, on the other hand, are in line with the values that can be found in the literature [41, 42]. Analyzing the broad set of data collected by Work and Lian [13] and Pervier et al. [43], dynamic methods generally show lower ice adhesion values than static ones. The effect of the stress concentrations on the static method, together with the different nature of the measurement methods, could explain this discrepancy. Note that the standard deviations obtained for each set of tests are in the range of 10-20%. Therefore, if considered individually, repeatable results are achieved for both methods and substrates. As previously mentioned, the low-fiction coating was expected to have lower ice adhesion than the bare one. However, data show that shear strength values in both static and dynamic conditions are similar to those for bare titanium. This value cannot be explained by the roughness values, as the roughness of the coated plate is lower than that of the uncoated sample. High value of ice adhesion may be related to the coating surface chemistry. In particular, the content of silicon might be detrimental to ice adhesion, meaning that low friction does not correlate necessarily to low ice adhesion. More studies need to be conducted on silicon-based coatings to validate this hypothesis.

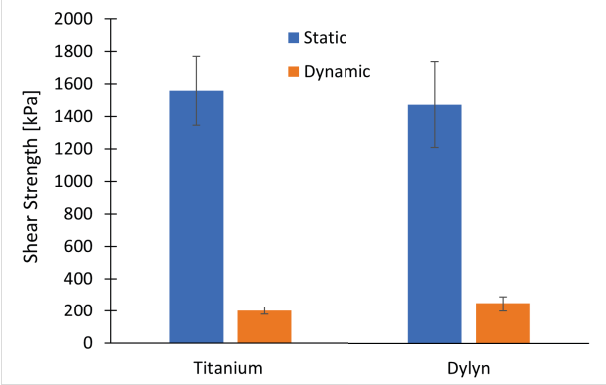

Figure 9: Comparison between average shear strength values of bare titanium and Dylyn coated titanium. Both substrates have been tested with dynamic and static test methods.

Conclusions

This study compares two different shear strength measurement techniques: (i) a dynamic, vibratory approach and (ii) a more traditional static push test on a horizontal surface. The dynamic approach is based on the excitation of a selected resonant frequency that causes pure adhesive detachment of ice. The same dynamic conditions are computed in a numerical simulation, which is used to retrieve the shear strength. The static method consists in a standard horizontal push test, where particular attention is given to the loading condition of the ice column to ensure pure shear stress detachment at the ice-substrate interface. The maximum applied force at the moment of adhesive failure is divided by the projected ice-substrate contact area to calculate the ice adhesion strength.

Two substrates have been tested: a bare titanium alloy plate and another with the Oerlikon Dylyn low-friction coating. The results between the two measurement methods are very different, by a factor 6/6.8. On one hand, for the dynamic measurements, similar values for ice adhesion on bare titanium are found in [41, 42]. Also, divergence between static and dynamic test methods is suggested by literature studies. In particular, dynamic methods generally show lower ice adhesion values than static ones [13], [43]. As such, more tests are needed to understand if the use of the average shear strength for static push test leads to an incorrect overestimation of the critical shear strength. In addition, the heating of the samples induced by the vibration has to be investigated further. It was seen in [42] that an increase in temperature during testing with rotor-blade centrifugal test results in a decrease of the ice adhesion. Hence, thermal effects could contribute to lower the shear strength of the dynamic test.

The lower roughness of the low-friction coating did not result in lower ice adhesion. The components constituting the coating, such as silicon, could be responsible for the increased ice adhesion. However, more studies on silicon-based coatings and with different surface treatments are needed for the validation of this hypothesis. As such, this study represents a first attempt to establish a new experimental framework and to facilitate the correlation of different ice adhesion test methods.

At the time this study was performed, no low ice adhesion coatings were available. This work will be extended by comparing different low-adhesion coatings using the methodology discussed here.

References

1. T. Laakso, H. Holttinen, G. Ronsten, L. Tallhaug, R. Horbaty, I. Baring-Gould, A. Lacroix, E. Peltola, and B. Tammelin, "State-of-the-art of wind energy in cold climates," *IEA annex XIX*, vol. 24, p. 53, 2003.

2. L. Gao, T. Tao, Y. Liu, and H. Hu, "A field study of ice accretion and its effects on the power production of utility-scale wind turbines," *Renewable energy*, vol. 167, pp. 917–928, 2021.

3. J.-L. Laforte, M. Allaire, and J. Laflamme, "State-of-the-art on power line de-icing," *Atmospheric Research*, vol. 46, no. 1-2, pp. 143–158, 1998.

4. R. W. Gent, N. P. Dart, and J. T. Cansdale, "Aircraft icing," *Philosophical Transactions of the Royal Society of London. Series A: Mathematical, Physical and Engineering Sciences*, vol. 358, no. 1776, pp. 2873–2911, 2000.

5. F. T. Lynch and A. Khodadoust, "Effects of ice accretions on aircraft aerodynamics," *Progress in Aerospace Sciences*, vol. 37, no. 8, pp. 669–767, 2001.

6. S. K. Thomas, R. P. Cassoni, and C. D. MacArthur, "Aircraft anti-icing and de-icing techniques and modeling," *Journal of aircraft*, vol. 33, no. 5, pp. 841–854, 1996.

7. Z. Goraj, "An overview of the deicing and anti-icing technologies with prospects for the future," in *24th international congress of the aeronautical sciences*, vol. 29, 2004.

8. T. Bai, C. Zhu, B. Miao, K. Li, and C. Zhu, "Vibration de-icing method with piezoelectric actuators," *Journal of Vibroengineering*, vol. 17, no. 1, pp. 61–73, 2015.

9. E. Villeneuve, D. Harvey, D. Zimcik, R. Aubert, and J. Perron, "Piezoelectric deicing system for rotorcraft," *Journal of the American Helicopter Society*, vol. 60, no. 4, pp. 1–12, 2015.

10. V. Pommier-Budinger, M. Budinger, P. Rouset, F. Dezitter, F. Huet, M. Wetterwald, and E. Bonaccurso, "Electromechanical resonant ice protection systems: initiation of fractures with piezoelectric actuators," *AIAA Journal*, vol. 56, no. 11, pp. 4400–4411, 2018.

11. M. Farzaneh and W. A. Chisholm, "Protective coatings for overhead lines in winter conditions," in *Techniques for Protecting Overhead Lines in Winter Conditions*, pp. 195–309, Springer, 2022.

12. I. Tagliaro, A. Cerpelloni, V.-M. Nikiforidis, R. Pillai, and C. Antonini, "On the development of icephobic surfaces: Bridging experiments and simulations," in *The Surface Wettability Effect on Phase Change*, pp. 235–272, Springer, 2022.

13. A. Work and Y. Lian, "A critical review of the measurement of ice adhesion to solid substrates," *Progress in Aerospace Sciences*, vol. 98, pp. 1–26, 2018.

14. S. Tarquini, C. Antonini, A. Amirfazli, M. Marengo, and J. Palacios, "Investigation of ice shedding properties of superhydrophobic coatings on helicopter blades," *Cold regions science and technology*, vol. 100, pp. 50–58, 2014.

15. S. Rønneberg, C. Laforte, C. Volat, J. He, and Z. Zhang, "The effect of ice type on ice adhesion," *AIP advances*, vol. 9, no. 5, p. 055304, 2019.

16. S. Rønneberg, J. He, and Z. Zhang, "The need for standards in low ice adhesion surface research: a critical review," *Journal of adhesion science and technology*, vol. 34, no. 3, pp. 319–347, 2020.

17. K. Golovin, S. P. Kobaku, D. H. Lee, E. T. DiLoreto, J. M. Mabry, and A. Tuteja, "Designing durable icephobic surfaces," *Science advances*, vol. 2, no. 3, p. e1501496, 2016.

18. K. Golovin, A. Dhyani, M. Thouless, and A. Tuteja, "Low–interfacial toughness materials for effective large-scale deicing," *Science*, vol. 364, no. 6438, pp. 371–375, 2019.

19. E. J. Y. Ling, V. Uong, J.-S. Renault-Crispo, A.-M. Kietzig, and P. Servio, "Reducing ice adhesion on nonsmooth metallic surfaces: wettability and topography effects," *ACS applied materials & interfaces*, vol. 8, no. 13, pp. 8789–8800, 2016.

20. Z. He, Y. Zhuo, F. Wang, J. He, and Z. Zhang, "Design and preparation of icephobic pdms-based coatings by introducing an aqueous lubricating layer and macro-crack initiators at the ice-substrate interface," *Progress in Organic Coatings*, vol. 147, p. 105737, 2020.

21. Z. He, S. Xiao, H. Gao, J. He, and Z. Zhang, "Multiscale crack initiator promoted super-low ice adhesion surfaces," *Soft matter*, vol. 13, no. 37, pp. 6562–6568, 2017.

22. C. Wang, W. Zhang, A. Siva, D. Tiea, and K. J. Wynne, "Laboratory test for ice adhesion strength using commercial instrumentation," *Langmuir*, vol. 30, no. 2, pp. 540–547, 2014.

23. V. F. Petrenko and S. Peng, "Reduction of ice adhesion to metal by using self-assembling monolayers (sams)," *Canadian journal of physics*, vol. 81, no. 1-2, pp. 387–393, 2003.

24. L. Raraty and D. Tabor, "The adhesion and strength properties of ice," *Proceedings of the Royal Society of London. Series A. Mathematical and Physical Sciences*, vol. 245, no. 1241, pp. 184–201, 1958.

25. R. Haehnel and N. Mulherin, "The bond strength of an ice–solid interface loaded in shear," *Ice in Surface Waters, Shen, Rotterdam*, pp. 597–604, 1998.

26. T. Bharathidasan, S. V. Kumar, M. Bobji, R. Chakradhar, and B. J. Basu, "Effect of wettability and surface roughness on ice-adhesion strength of hydrophilic, hydrophobic and superhydrophobic surfaces," *Applied surface science*, vol. 314, pp. 241–250, 2014.

27. T. Maitra, S. Jung, M. E. Giger, V. Kandrical, T. Ruesch, and D. Poulikakos, "Superhydrophobicity vs. ice adhesion: The quandary of robust icephobic surface design," *Advanced Materials Interfaces*, vol. 2, no. 16, p. 1500330, 2015.

28. F. T. Baheri, L. D. Poulikakos, D. Poulikakos, and T. Schutzius, "Ice adhesion behavior of heterogeneous bituminous surfaces," *Cold Regions Science and Technology*, vol. 192, p. 103405, 2021.

29. A. R. Lovell, G. R. Hoch, C. J. Donnelly, J. M. Hodge, R. B. Haehnel, and E. Asenath-Smith, "Shear and tensile delamination of ice from surfaces: The ice adhesion peel test (iapt)," 2021.

30. C. Laforte and A. Beisswenger, "Icephobic material centrifuge adhesion test," in *Proceedings of the 11th International Workshop on Atmospheric Icing of Structures, IWAIS, Montreal, QC, Canada*, pp. 12–16, 2005.

31. J. L. Palacios, Y. Han, E. W. Brouwers, and E. C. Smith, "Icing environment rotor test stand liquid water content measurement procedures and ice shape correlation," *Journal of the American Helicopter Society*, vol. 57, no. 2, pp. 29–40, 2012.

32. A. Laroche, M. J. Grasso, A. Dolatabadi, and E. Bonaccurso, "Tensile and shear test methods for quantifying the ice adhesion strength to a surface," *Ice Adhesion: Mechanism, Measurement and Mitigation*, pp. 237–284, 2020.

33. A. J. Meuler, J. D. Smith, K. K. Varanasi, J. M. Mabry, G. H. McKinley, and R. E. Cohen, "Relationships between water wettability and ice adhesion," *ACS applied materials & interfaces*, vol. 2, no. 11, pp. 3100–3110, 2010.

34. V. Palanque, E. Villeneuve, M. Budinger, V. Pommier-Budinger, and G. Momen, "Cohesive strength and fracture toughness of atmospheric ice," *Cold Regions Science and Technology*, vol. 204, p. 103679, 2022.

35. V. Palanque, E. Villeneuve, M. Budinger, V. Pommier-Budinger, and G. Momen, "Experimental measurement and expression of atmospheric ice young's modulus according to its density," *Available at SSRN 4120112*.

36. V. Palanque, M. Budinger, V. Pommier-Budinger, L. Bennani, and D. Delsart, "Electro-mechanical resonant ice protection systems: Power requirements for fractures initiation and propagation," in *AIAA Aviation 2021 Forum*, p. 2651, 2021.

37. G. Gastaldo, V. Palanque, M. Budinger, and V. Pommier-Budinger, "Stress and energy release rate influence on ice shedding with resonant electro-mechanical de-icing systems," in *ICAS 2022-33rd Congress of the International Council of the Aeronautical Sciences*, 2022.

38. J. D. Smith, A. J. Meuler, H. L. Bralower, R. Venkatesan, S. Subramanian, R. E. Cohen, G. H. McKinley, and K. K. Varanasi, "Hydrate-phobic surfaces: fundamental studies in clathrate hydrate adhesion reduction," *Physical Chemistry Chemical Physics*, vol. 14, no. 17, pp. 6013–6020, 2012.

39. D. Leguillon, "Strength or toughness? a criterion for crack onset at a notch," *European Journal of Mechanics-A/Solids*, vol. 21, no. 1, pp. 61–72, 2002.

40. E. Martin, T. Vandellos, D. Leguillon, and N. Carrère, "Initiation of edge debonding: coupled criterion versus cohesive zone model," *International Journal of Fracture*, vol. 199, pp. 157–168, 2016.

41. A. Laroche, D. Bottone, S. Seeger, and E. Bonaccurso, "Silicone nanofilaments grown on aircraft alloys for low ice adhesion," *Surface and Coatings Technology*, vol. 410, p. 126971, 2021.

42. J. Soltis, J. Palacios, T. Eden, and D. Wolfe, "Evaluation of ice-adhesion strength on erosion-resistant materials," *AIAA journal*, vol. 53, no. 7, pp. 1825–1835, 2015.

43. M. L. Pervier, B. G. Lerma, E. P. Moncholi, and D. Hammond, "A new test apparatus to measure the adhesive shear strength of impact ice on titanium 6al-4v alloy," *Engineering Fracture Mechanics*, vol. 214, pp. 212–222, 2019.

Contact Information

Luca Stendardo, Ph.D. candidate
luca.stendardo@unimib.it
Giulia Gastaldo, Ph.D. candidate
giulia.gastaldo@isae-supaero.fr

Author Contributions

†G.G and L.S. contributed equally.

All authors reviewed the results and approved the final version of the manuscript.

Acknowledgments

This project has received funding from the European Union's Horizon 2020 research and innovation programme under the Marie Skłodowska-Curie grant agreement No 956703 (SURFICE Smart surface design for efficient ice protection and control).

Definitions, Acronyms, Abbreviations

IPS	Ice Protection System
LWC	Liquid Water Content
MVD	Median Volumetric Diameter